Mixed-Mode Failure of Thin Films Using Laser-Generated Shear Waves

by J. Wang, N.R. Sottos, and R.L. Weaver

ABSTRACT—A new test method is developed for studying mixed-mode interfacial failure of thin films using laser generated stress waves. Guided by recent parametric studies of laser-induced tensile spallation, we successfully extend this technique to achieve mixed-mode loading conditions. By allowing an initial longitudinal wave to mode convert at an oblique surface, a high amplitude shear wave is generated in a fused silica substrate and propagated toward the thin-film surface. A shear wave is obtained with amplitude large enough to fail an Al film/fused silica interface and the corresponding shear stress calculated from high-speed interferometric displacement measurements. Examination of the interfaces failed under mixed-mode conditions reveals significant wrinkling and tearing of the film, in great contrast to blister patterns observed in similar Al films failed under tensile loading.

KEY WORDS—Mixed-mode, film failure, pulsing laser, shear wave, mode conversion, interfacial adhesion

Introduction

Interfacial adhesion is a critical parameter governing the mechanical properties and reliability of a thin film on a substrate. Significant effort has been devoted to the design and implementation of test procedures for the measurement of thin-film adhesion, of which the most common are the scratch, peel, pull, blister and indentation tests.[1–4] In all of these tests, the interface is subject to very high stress levels and consequent inhomogeneous deformations. Large amounts of plastic deformation can be present and dominate the behavior during the test.[5,6] The stress fields are difficult to analyze and the resulting adhesion measurements tend to be qualitative and comparative. Both the intrinsic work of adhesion and the work of plastic dissipation control thin-film interfacial failure strength. Experiments capable of characterizing the intrinsic interfacial strength, without any contribution from plastic dissipation, are therefore critical to obtaining a fundamental understanding of thin-film failure modes.

The laser spallation technique was introduced by Yang[7] and Vossen,[8] and later extended by Gupta and coworkers[9–14] to determine the intrinsic tensile strength of planar interfaces (Fig. 1). This technique overcomes many of the inadequacies of the adhesion tests described above and can be used to determine the intrinsic interfacial strength. In the laser spallation experiment, a high-energy laser pulse (duration of the order of nanoseconds) is absorbed by a thin metallic layer confined between a transparent backing and a substrate. Upon absorbing the laser energy, the sudden expansion of the confined layer generates a compressive stress wave directed towards the test film (deposited on the front surface of the substrate). Reflection of the compressive wave from the surface of the test film creates a tensile pulse, which leads to spalling of the test film. The stress pulse amplitude is inferred by measuring the out-of-plane displacement of the test film with a laser interferometer as developed by Barker and Hollenbach,[15] and interfacial strength is thereby obtained. The technique has been used to measure the tensile strength of a wide variety of metal/ceramic interfaces[11] and ceramic/ceramic interfaces.[12]

More recently, Wang et al.[16] carried out an extensive parametric study of the tensile spallation experiment. The spallation behavior of Al thin films was investigated as a function of substrate thickness, film thickness, laser energy and various parameters governing the source. Interface stress was found to increase with film thickness, but to decrease with substrate thickness due to geometric attenuation. Two different substrate materials, single-crystal Si (100) and fused silica, were considered. Of particular significance was the development of a decompression shock in the fused silica substrate, which is critical to the generation of the fast fall times needed for significant loading of thin film interfaces. This shock enhances the failure of thin-film interfaces, especially in thicker samples.

In all of the experiments reported to date, only normal pressure pulses were applied to the films. Consequently, the interfaces were subjected only to tensile (mode I) loading. In most commercial applications, however, thin-film interfaces fail under mixed-mode conditions.[17] Design of experiments to measure the interface debonding over a range of mode-mixity relevant to practical problems is a significant challenge. Several test methods for characterizing the mixed-mode interfacial fracture of a bilayer have been proposed, such as mixed-mode double cantilever beam,[18] double cantilever drilled compression,[17] mixed-mode flexure,[19] and Brazil-nut specimen.[20] Most of these test methods involve sandwich configurations produced by diffusion bonding at relatively high homologous temperatures and are thus restricted to certain types of interfaces. Measurement using these sandwiches is even more problematic for thin film interfaces produced at relatively low temperatures (by, for

J. Wang (wang@engr.ucr.edu) is an Assistant Professor, Department of Mechanical Engineering, University of California, Riverside, CA 92521. N.R. Sottos (SEM Member) and R.L. Weaver are Professors, Department of Theoretical and Applied Mechanics, University of Illinois at Urbana-Champaign, 216 Talbot Lab, 104 S. Wright St., Urbana, IL 61801.

Original manuscript submitted: January 24, 2003.
Final manuscript received: January 24, 2003.

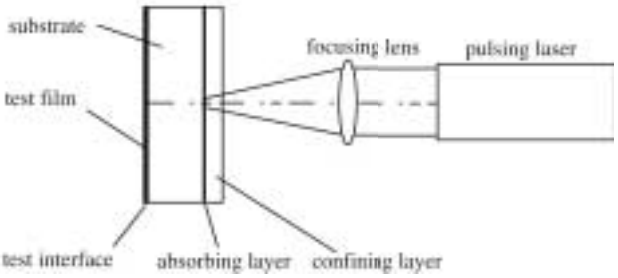

Fig. 1—Schematic diagram of the tensile laser spallation experiment[9,14]

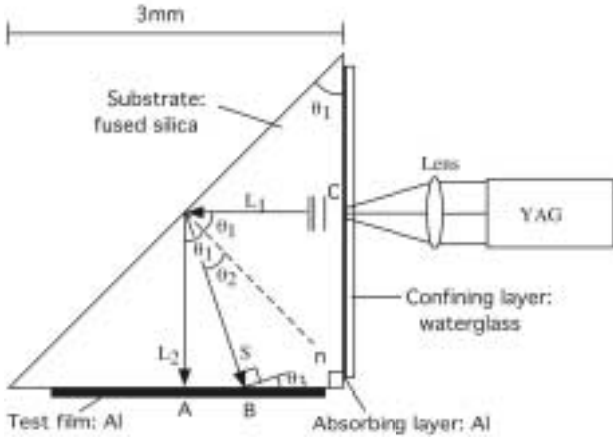

Fig. 2—Configuration for laser generated shear waves

example, sputtering or evaporation) due to difficulty loading the film in a controlled manner at the relevant phase angle.[17]

In this paper, we present a new test method for studying the mixed-mode interfacial failure of thin films using laser generated stress waves. Guided by recent parametric studies of the tensile spallation test[16] as well as previous researchers' work,[8,9–14] we successfully extend this technique to achieve mixed-mode loading conditions.

Experimental Method

Mixed-mode loading is accomplished by modifying the sample geometry so that a high strain rate shear wave is generated by mode conversion at an oblique surface and then allowed to impinge upon the test film. A diagram describing the generation of high-amplitude, short-duration-shear-waves is shown in Fig. 2. Similar to the tensile spallation experiment, the sample consists of a transparent confining layer, a thin energy-absorbing layer, a substrate and a test film. In order to generate a high amplitude shear wave, the planar substrate in the tensile spallation is replaced with a triangular prism. An infrared, Nd:YAG pulse (λ = 1064 nm) with a variable energy content between 1 and 110 mJ is incident on the absorbing layer at point C. The shape of the laser pulse fits well to a Gaussian distribution of the form, $I(t) = I_0 \exp(-t^2/T^2)$, where I_0 = 18.9 mJ ns^{-1} at full power and T = 2.9 ns. The energy-absorbing layer is chosen to be much thicker than the critical penetration depth of laser light at this wavelength. Under this consideration, the laser energy is deposited at the interface of the confining layer and the energy-absorbing layer. The YAG pulse does not penetrate the substrate. The nominal diameter of the YAG laser beam is 3.5 mm. In order to increase the laser fluence, the laser beam is focused to a 1 mm diameter spot on the energy-absorbing layer. When the laser pulse reaches the absorbing layer, a longitudinal compressive stress wave, L_1, of rise time comparable to that of the laser pulse is emitted from the absorbing layer. The wave that propagates into the triangular block is reflected at the oblique surface, and a major fraction of its energy (the exact amount depends on details of the angle θ_1 and the material elastic constants) is mode converted into a shear wave, S. A smaller amount reflects as a longitudinal wave, L_2. The two reflected waves are then incident (propagation direction depends on the precise choice of θ_1) upon the test film surface at points A and B, respectively.

Figure 2 shows the angles θ_1 and θ_2 between the normal to the oblique surface, *n*, and the propagation directions of the longitudinal and shear waves; θ_3 is the angle between the shear wave displacement (displacement is normal to the propagation direction of the shear wave) and the test film: $\theta_3 = \theta_1 - \theta_2$. We denote the displacement amplitudes of the incident longitudinal, reflected longitudinal and shear waves with u_{L_1}, u_{L_2} and u_S. According to standard wave propagation theory,[21] the amplitude ratios are expressed as

$$\frac{u_{L_2}}{u_{L_1}} = \frac{\sin 2\theta_1 \sin 2\theta_2 - k^2 \cos^2 2\theta_2}{\sin 2\theta_1 \sin 2\theta_2 + k^2 \cos^2 2\theta_2} \tag{1}$$

$$\frac{u_S}{u_{L_1}} = \frac{2k \sin 2\theta_1 \cos 2\theta_2}{\sin 2\theta_1 \sin 2\theta_2 + k^2 \cos^2 2\theta_2} \tag{2}$$

where $k = c_L/c_s$ is the ratio of longitudinal and shear wave speeds, and θ_2 is given by Snell's law

$$\sin\theta_1 / \sin\theta_2 = k. \tag{3}$$

Based on our recent parametric study of tensile spallation,[16] fused silica (GE type 124) is chosen as the substrate material, waterglass as the confining layer, and Al as both absorbing material and test film. The longitudinal wave speed for the substrate is c_L = (5.9407 ± 0.0004) × 10^3 m s^{-1} as measured on a prism using waves traveling between the parallel surfaces. A shear wave speed of c_S = 3.75 × 10^3 m s^{-1} is taken from the manufacture's reference provided by Integrated Optics Service Co., as is the density ρ = 2.2 × 10^3 kg m^{-3}. For this specific material, $k \approx 1.584$.

In Fig. 3, the displacement amplitude ratios (1) and (2) are plotted as a function of incident angle θ_1. At an incident angle $\theta_1 = 45°$, the coefficient of mode conversion from incident longitudinal wave L_1 to shear wave S is nearly at a maximum, i.e., most of the energy of the incident longitudinal wave, L_1, is mode converted into the shear wave, S. Thus, for our purposes, the convenient specimen angle $\theta_1 = 45°$ is also optimal for the generation of high amplitude shear waves. From eq (3), the angle of the reflected shear wave is found to be $\theta_2 = 26.5°$, so $\theta_3 = 18.5°$. In this configuration, the reflected longitudinal wave will be incident at point A normal to the test film surface and all of the amplitude of the longitudinal displacement will contribute to the

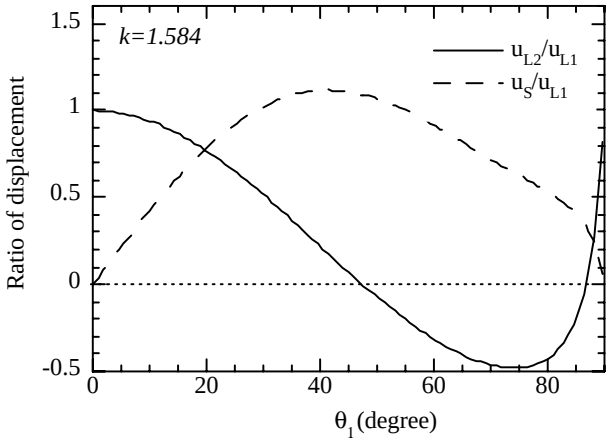

Fig. 3—Ratio of wave displacement amplitudes as function of incident angle θ_1

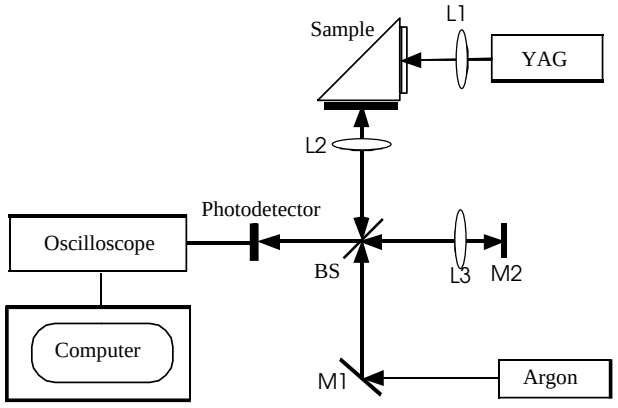

Fig. 4—Schematic diagram of the mixed-mode loading experiment and interferometric displacement measurement

measured out-of-plane motion at point A. The corresponding shear wave arrives at the test film surface at point B, where about one-third ($\sin\theta_3 = 0.317$) of the shear wave displacement contributes to the out-of-plane motion. The distance between points A and B is determined by the size of the sample and specific incident position of the YAG laser. Guided by the previous analytical analysis of wave attenuation with regard to substrate thickness,[16] the lengths of the orthogonal sides of the triangular cross-section in Fig. 2 are chosen to be 3 mm. Assuming the YAG beam is incident at the center of the 3 mm wide absorbing layer surface, the distance between points A and B is found to be approximately 0.5 mm. However, for a 1 mm diameter YAG spot, the diameter of the wave front of the longitudinal wave will also be 1 mm (centered at point A) and the diameter of the wave front of the shear wave will be slightly larger, about 1.33 mm (centered at point B). Thus, within region AB, the signals from the reflected longitudinal and shear waves are overlapped, although they arrive at different times.

A Michelson interferometer is used for the displacement measurement as shown in Fig. 4. Two identical short focal distance lenses L2 and L3 are placed 20 mm away from the sample and stationary mirror in order to obtain a small focal spot ($\sim$10 μm). In the tensile spallation experiment, every point within the argon laser detection spot is in the same phase of motion, thus the spot size of the argon beam is not critical. In the shear test, however, each point within the detection window has a different arrival time, so a smaller argon laser detection spot will better resolve the fastest feature in the stress wave.

When using the interferometer to measure out-of-plane displacement, the argon beam can be focused anywhere between points A and B and the interferometer will detect both the longitudinal L_2 and shear waves S. The arrival time difference for the two waves depends on where the YAG laser beam is aimed, but is over 100 ns. Previous results obtained on a 3 mm thick fused silica plate sample[16] indicate that the maximum stress is achieved within 30 ns after the initial wave arrival. By the time the shear wave arrives in the current experiment, the weaker longitudinal stress wave has already passed and the tail of that stress is almost negligible. Therefore, the important parts of the interferometric signals due to the longitudinal and shear waves are expected to be distinguishable.

Measuring Principles

A detailed description of the Michelson interferometer is provided elsewhere.[16] Any out-of-plane motion of the sample surface causes a change in signal frequency due to the Doppler effect. A full fringe corresponds to half wavelength ($\lambda/2 = 257$ ns) out-of-plane movement. By focusing the argon detection beam at a point between A and B (Fig. 2), a longitudinal wave, L_2, and a shear wave, S, will be detected. The normal displacement u_{L_2} is obtained directly from the out-of-plane interferometric measurements at point A. The shear displacement amplitude u_s can then be calculated from u_{L_2} using the mode conversion coefficients in eqs (1) and (2):

$$\frac{u_S}{u_{L_2}} = \frac{2k \sin 2\theta_1 \cos 2\theta_2}{\sin 2\theta_1 \sin 2\theta_2 - k^2 \cos^2 2\theta_2}. \tag{4}$$

Alternatively, the value of u_s can also be obtained from the shear part of the interferometric measurement at point B. Ideally, these two methods should give the same results. Note that, in the experiment, the wave displacements u_s and u_{L_2} in the substrate are not measured directly, rather the out-of-plane displacements of the film, $2u_s\beta \sin\theta_3$ and $2u_{L_2}$, are actually measured, where β is a factor due to a second mode conversion when shear wave S reaches the free surface at point B, β = 1.23. Once the displacements are obtained, the corresponding stresses in the substrate and at the interface are calculated

$$\sigma^{L_2}_{substrate} = -(\rho c_L)_{substrate} \frac{\partial u_{L_2}}{\partial t}, \tag{5}$$

$$\tau^{S}_{substrate} = -(\rho c_s)_{substrate} \frac{\partial u_S}{\partial t}, \tag{6}$$

$$\sigma^{L_2}_{interface} = -2(\rho h)_{film} \frac{\partial^2 u_{L_2}}{\partial t^2}, \tag{7}$$

$$\tau^{S}_{interface} = -2(\rho h)_{film}\frac{\partial^2 u_S \gamma \cos\theta_3}{\partial t^2}, \quad (8)$$

$$\sigma^{S}_{interface} = -2(\rho h)_{film}\frac{\partial^2 u_S \beta \sin\theta_3}{\partial t^2}, \quad (9)$$

where h is the test film thickness, $\sigma^{L_2}_{substrate}$ and $\tau^{s}_{substrate}$ are the normal and shear stress amplitudes of the waves in the substrate, $\sigma^{L_2}_{interface}$ is the interface tensile stress induced by the longitudinal wave L_2 at point A (Fig. 2), $\tau^{s}_{interface}$ is the interface shear stress induced by the shear wave S at point B, $\sigma^{S}_{interface}$ is the interface tensile stress induced by the shear wave S at point B (Fig. 2), and γ is also a factor due to the second mode conversion when shear wave S reaches point B and $\gamma = 0.94$.

Equations (8) and (9) indicate that both normal and shear stresses exist at point B and thus the film interface in this region is actually under mixed-mode loading. For the current sample dimensions, however, the shear stress is much higher than the normal stress ($\tau^{S}_{interface}/\sigma^{S}_{interface} \approx 2.3$). In order to obtain a pure shear-mode loading, the sample shown in Fig. 2 needs to be cut perpendicular to the propagation direction of shear wave S around point B. Alternatively, θ_1 could be chosen to be greater.

Sample Preparation and Alignment

Figure 5 shows a schematic diagram of the prismatic sample used for the mixed-mode loading experiment. The length of the prism is chosen to be 15 mm based on the translation extent of our mounting stage. When preparing the sample, the Al test film and absorbing layer are vapor deposited at the top and bottom sections of the two orthogonal surfaces of the prism, each with an area of 6×3 mm^2. In the middle section of the sample, two windows of 3×3 mm^2 are left for the purpose of alignment. The vacuum level of the evaporator is controlled around 4.0×10^{-6} Torr and the deposition rate is held between 10–15 Å s^{-1}. The final thickness for the absorbing layer is controlled at 0.4 μm while the test film thickness may vary between experiments.

For alignment of the lasers, a very thin Al film is deposited at the oblique surface of the middle prism section with the two orthogonal surfaces left transparent. As pictured in Fig. 5, the argon laser is incident normal to the window on the test film surface and reflected out of the window on the absorbing layer surface. A YAG sensitive paper is then placed in front of the window on the absorbing layer surface. By carefully adjusting the position of the sample and YAG laser, the argon laser and YAG laser can be well aligned. Because the longitudinal waves L_1 and L_2 follow the same path as the lasers, this alignment method provides a good match between the arrival position of the longitudinal wave L_2 and the argon detection spot. In order to align the arrival position of the shear wave S and the argon laser, we only need to move the argon laser horizontally by a theoretically known distance (0.5 mm for current geometry). Since moving the argon laser can complicate the alignment, the sample is translated instead to the opposite direction for the same distance. After the alignment is complete, a thin waterglass confining layer is then put on the absorbing layer side of the sample. During the experiment, the sample is moved vertically for multiple tests. The current geometry allows up to four tests per sample.

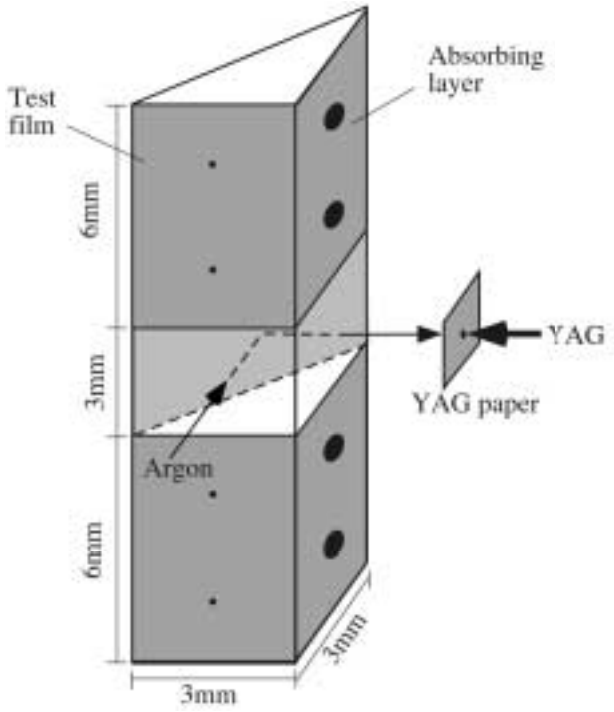

Fig. 5—Sample schematic diagram for mixed-mode experiment

Experimental Results

Experiments were carried out on samples with an Al test film thickness of 0.5–1.0 μm. A typical interferometric signal at point A is shown in Fig. 6. Based on the material properties provided earlier and the travel distance of 3 mm, the arrival of the longitudinal wave L_2 is expected at about 585 ns (3.0 mm/5.94 mm μs^{-1} plus 80 ns delay between the Q-switch trigger and the firing of the YAG). The arrival of the shear wave S at point A is expected at about 710 ns. Each arrival time is referenced to the trigger time of the Q-switch of the YAG laser ($t = 0$). The interferometric signal in Fig. 6 shows the expected longitudinal and shear arrivals at t_2 = 600 ns and t_3 = 710 ns, respectively. A shock appears to arrive at t_4 = 780 ns (indicated by the sudden turning in the fringe signal), but interpretation is difficult since point A is not the center of shear arrival and the arrival is much later than the expected 740 ns (30 ns after the initial shear wave arrival). The data also reveal the arrival of a low amplitude stress at about t_1 = 408 ns, much earlier than the expected longitudinal wave L_2. This arrival time is approximately equal to the travel time of a longitudinal wave from a point 0.25 mm below C to A in the triangular prism (Fig. 2).

In order to confirm the observed wave arrivals and to evaluate the effect of diagonally generated stress waves from C to A (Fig. 2), a reference experiment was carried out on a much larger prism with cross-section dimensions of 15×15 mm^2 as shown in Fig. 7. The Nd:YAG laser was incident at point C* on the absorbing layer at a distance of 1.5 mm from the bottom surface and the argon laser was focused at a point A* 1.5 mm away from the right surface (same distance as in the smaller 3×3 mm^2 samples). In this configuration, waves reflected from the oblique surface only arrived at positions

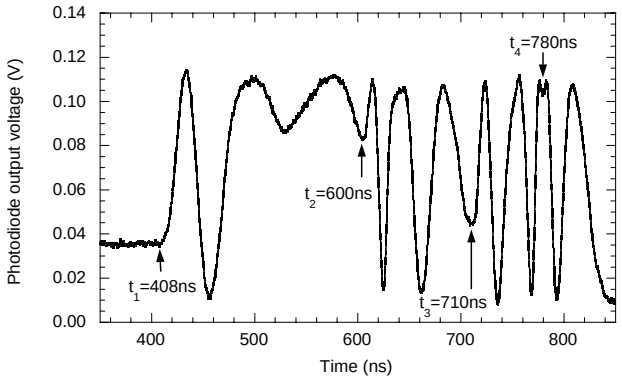

Fig. 6—Typical interferometric signal obtained in mixed-mode loading experiment at point A

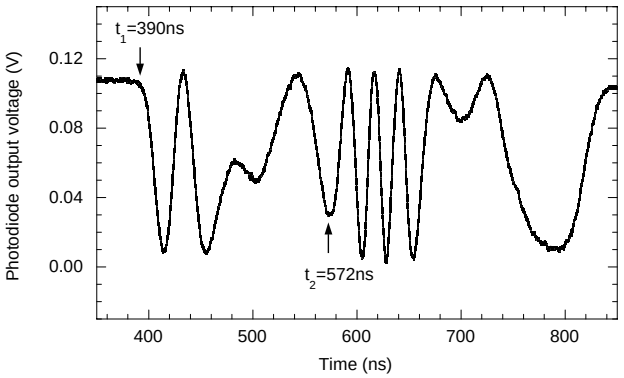

Fig. 8—Interferometric signal detected at point A* for diagonal wave evaluation

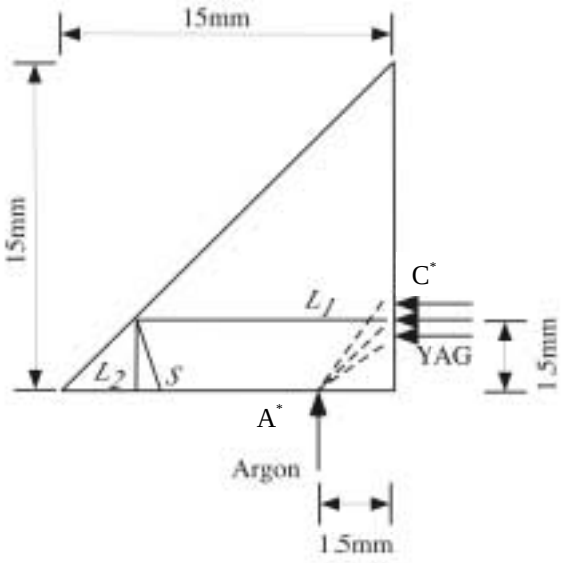

Fig. 7—Schematic diagram of the reference experiment for diagonal wave evaluation

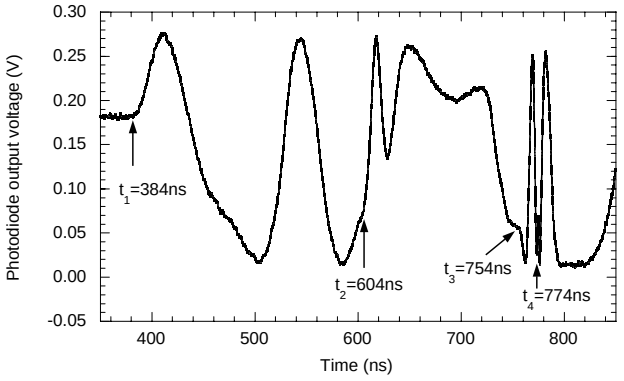

Fig. 9—Typical interferometric signal obtained on a 1.0 μm thick Al film at point B

far to the left of point A*, and the signal detected at A* was solely due to diagonal waves propagated directly from point C*.

The interferometric signal detected from point A* is shown in Fig. 8. The signal shows two comparatively strong wave arrivals. As expected from a diagonally generated longitudinal wave from C* to A*, the first wave arrival is at t_1 = 390 ns. There is also a clear second wave arrival at t_2 = 572 ns. The ratio between the first wave arrival time t_1 = 390 ns and the second at t_2 = 572 ns is approximately equal to the ratio between the longitudinal and shear wave speeds c_L and c_S, i.e.,

$$\frac{t_2 - 80\text{ ns}}{t_1 - 80\text{ ns}} = \frac{572\text{ ns} - 80\text{ ns}}{390\text{ ns} - 80\text{ ns}} = 1.587 \approx \frac{c_L}{c_S} = \frac{5.94}{3.75} = 1.584. \quad (10)$$

The results of this reference experiment indicate that in the mixed-mode loading experiment of Fig. 2, a diagonally generated longitudinal wave will arrive before L_2 at approximately t_1 = 390 ns and a diagonally generated shear wave will arrive at t_2 = 572 ns (the same time as L_2). The additional diagonal waves are likely due to surface roughness of the confining layer at point C (Fig. 2), or sharp edges in the YAG beam. While the stress caused by the diagonal longitudinal wave is clearly quite low, the diagonal shear wave is much stronger than the L_2 wave. Since these two waves are overlapped, extracting information from the longitudinal wave L_2 signal is not reliable. Fig. 8 also shows that the diagonal waves become weak after 700 ns (indicated by the wide spacing of the interferometric fringes). Therefore, the shear part of the interferometric signal in the 3 mm prism can still be used to calculate the displacement of the shear wave.

To better quantify the interfacial stress at film failure, the argon detection beam was focused at point B (Fig. 2), the center of shear wave arrival. Figure 9 shows typical interferometric data obtained on a 1.0 μm thick Al film at point B at 60% of the full YAG power (~0.14 J mm^{-2}). Based on the geometry of the sample and the wave speeds in fused silica, we expect to see the shear wave arrival at point B 754 ns after firing the Q-switch of the YAG laser. The diagonally generated longitudinal and shear waves arrive at t_1 = 384 ns and t_2 = 604 ns, respectively. The shear wave S arrives at t_3 = 754 ns, the expected time.

An expanded view of the shear wave signal in Fig. 9 is shown in Fig. 10(a). The signal clearly shows tightening of

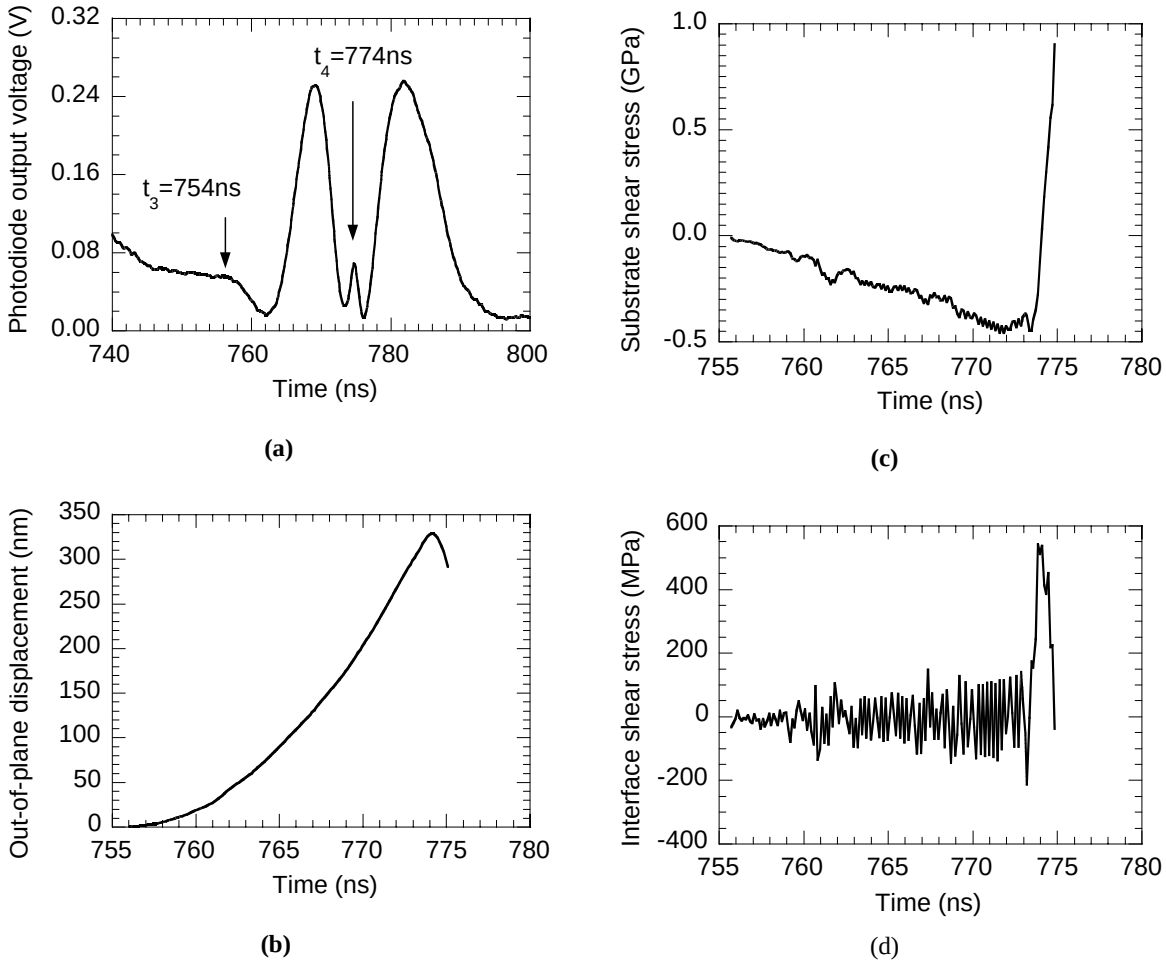

Fig. 10—Interferometric measurements obtained on a 1.0 μm thick Al film at point B: (a) fringe data (expanded view of the shear wave signal in Fig. 9); (b) out-of-plane displacement; (c) substrate shear stress, $\tau^s_{substrate}$ (d) interface shear stress, $\tau^s_{interface}$

fringe spacing (indicating acceleration in wave velocity) and a sudden turning at t_4 = 774 ns. The out-of-plane displacement is obtained from the voltage by fringe counting, as described in Wang et al.[16] (one full fringe corresponds to half-wavelength out-of-plane displacement), and is shown in Fig. 10(b). These displacements are identified as associated with shear wave *S* by their times of arrival. The data processing associated with the shear wave arrival is taken from the fringe data near t_4. The substrate and interface shear stress are calculated from the displacement using eqs (6) and (8) and shown in Figs. 10(c) and (d), respectively. Due to the acceleration in the fringe signal and the sudden turning in direction, a linear ramp is formed in the substrate stress profile with a peak stress of 0.47 GPa and followed by a sharp shock right before the turning. The stress profile is similar to that observed for shocks in our previous tensile experiment on the same material system[16] and also consistent with the shock profile described by Barker and Hollenbach.[22] After mode converting at the oblique surface, the stress wave has retained the characteristics of the shock developed in the initial longitudinal propagation L_1. The development of the shock is due to the nonlinear elasticity of the fused silica substrate and it greatly enhances the loading at the film interface. The maximum interface shear stress resulting from the shock is 537 MPa. The noise in Figs. 10(c) and (d) is due to the numerical differentiation of the displacement profile. The typical noise level is less than 10% of the measured maximum substrate stress and 20% of measured maximum interface stress. The associated tensile stress (not shown in Fig. 10) is 233 MPa as calculated from eq (9).

At the stress level reported in Fig. 10, a small amount of film failure was initiated (indicated by slight wrinkling at the edge of the loading spot). Significant damage, however, is observed when the films are tested under higher YAG laser power. Figure 11 shows two optical microphotographs of a 1.0 mm thick damaged film near point B at 80% and 100% of the full YAG power, respectively. That the film has failed in shear is clear. The film damage and failure mode are significantly different than observed for the tensile film spallation. In the shear case, the failed film is wrinkled and torn in sections. While under tensile loading the film was lifted off the surface in a blister-like fashion.[16] The direction of the wrinkling in Fig. 11 provides additional evidence that the failure is caused by a shear wave.

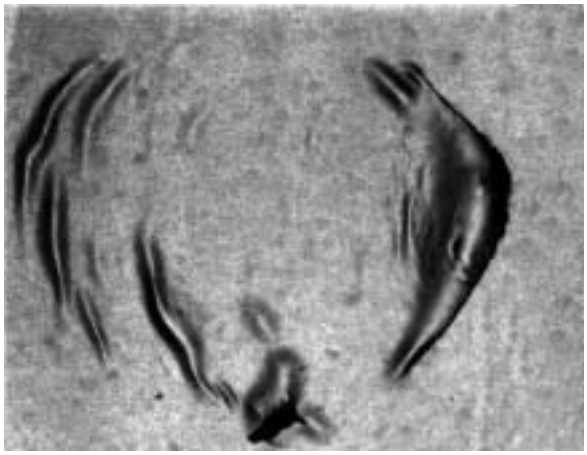

(a)

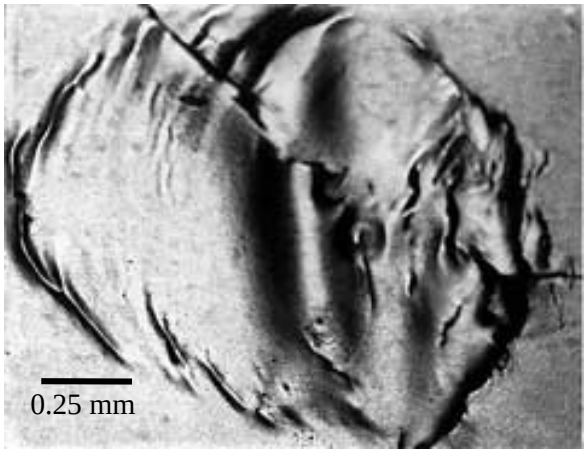

(b)

Fig. 11—Typical damage patterns observed on a 1.0 μm thick Al film at point B: (a) lower laser fluence (~0.112 J mm^{-2}); (b) higher laser fluence (~0.140 J mm^{-2}). The horizontal direction in the microphotograph here corresponds to the direction A → B of Fig. 2. B is at the center of the damage, A is to the left.

Interferometric measurements performed on three film thicknesses, 0.68, 0.8, and 1.0 mm, revealed an average interfacial shear strength (stress at failure initiation) of 523 ± 52 MPa[23] and an associated tensile stress of 227 ± 27 MPa. The error bar is the standard deviation from eight measurements. Failure initiation was determined by gradually increasing the YAG laser power until a small amount of damage was observed for each film thickness. The shear strength is slightly higher than the tensile strength of the same interface measured under pure tensile loading, which is about 490 MPa.[23]

Conclusions

A new test method was developed for studying mixed-mode interfacial failure of thin films using laser generated stress waves. A shear wave was generated with amplitude large enough to fail an Al film/fused silica interface and the resulting shear stress was calculated from high-speed interferometric displacement measurements. The interferometric fringe data revealed the development of a shock due to nonlinear softening of the fused silica substrate. After mode converting at the oblique surface, the stress wave retains features of the shock, similar to those observed in previous tensile experiments.[16] Quantitative data indicate that the interfacial strength in shear is about 523 MPa, which is slightly higher than the tensile strength obtained for the same interface under pure tensile loading.[23]

The failure patterns developed under mixed-mode loading (mostly shear mode) are different from those observed in the tensile spallation experiment. Significant wrinkling and tearing occurs in the films due to the shear loading. The current film failures also differ from other mechanisms reported in the literature such as film cracking due to residual tension and blister-like buckle driven delamination due to residual compression.[24] These preliminary results indicate that mode dependence of interfacial toughness plays a critical role in determining the sequence of events leading to film failure. The use of laser generated shear waves provides a new tool to explore a range of thin-film interfacial failure modes as well as the role of extrinsic effects such as residual stress, surface roughness, and imperfections.

Acknowledgments

The authors gratefully acknowledge the support of the National Science Foundation (CMS-99-88127). We would also like to acknowledge the use of the Frederick Seitz Materials Research Lab facilities at the University of Illinois.

References

1. Mittal, K.L., "Selected Bibliography on Adhesion Measurement of Films and Coatings," J. Adhesion Sci. Technol., **1** *(3), 247–259 (1987).*

2. Hull, T.R., Colligon, J.S., and Hill, A.E., "Measurement of Thin Film Adhesion," Vacuum, **37**, *327–330 (1987).*

3. Kriese, M.D., Gerberich, W.W., and Moody, N.R., "Quantitative Adhesion Measures of Multilayer Films: Part I. Indentation Mechanics," J. Mater. Res., **14** *(7), 3007–3018 (1999).*

4. Kriese, M.D., Gerberich, W.W., and Moody, N.R., "Quantitative Adhesion Measures of Multilayer Films: Part II. Indentation of W/Cu, W/W, Cr/W," J. Mater. Res., **14** *(7), 3019–3026 (1999).*

5. Kim, K.S. and Kim, J., "Elasto–plastic Analysis of the Peel Test for Thin Film Adhesion," J. Eng. Mater. Technol.-Trans. ASME, **110** *(3), 266–273 (1988).*

6. Thouless, M.D., "Fracture Mechanics for Thin Film Adhesion," IBM J. Res. Dev., **38**, *367–377 (1994).*

7. Vossen, J.L., "Measurement of Film–substrate Bond Strength by Laser Spallation," Adhesion Measurement of Thin Films, Thick Films and Bulk Coatings, ASTM STP **640**, *122–133 (1978).*

8. Yang, L.C., "Stress Waves Generated in Thin Metallic Films by a Q-swithed Ruby Laser," J. Appl. Phys., **45** *(6), 2601–2607 (1974).*

9. Gupta, V., Argon, A.S., Cornie, J.A., and Parks, D.M., "Measurement of Interface Strength by Laser Pulse-induced Spallation," Mater. Sci. Eng. A, **126**, *105–117 (1990).*

10. Gupta, V., Argon, A.S., Parks, D.M., and Cornie, J.A., "Measurement of Interface Strength by a Laser Spallation Technique," J. Mech. Phys. Solids, **40**, *141–180 (1992).*

11. Gupta, V. and Yuan, J., "Measurement of Interface Strength by the Modified Laser Spallation Technique. II. Applications to Metal/ceramic Interfaces," J. Appl. Phys., **74**, *2397–2404 (1993).*

12. Gupta, V., Yuan, J., and Pronin, A., "Recent Developments in the Laser Spallation Technique to Measure the Interface Strength and Its Relationship to Interface Toughness with Applications to Metal/ceramic, Ceramic/ceramic and Ceramic/polymer Interfaces," J. Adhesion Sci. Technol., **8**, *713–747 (1994).*

13. Yuan, J. and Gupta, V., "Measurement of Interface Strength by the Modified Laser Spallation Technique. I. Experiment and Simulation of the Spallation Process," J. Appl. Phys., **74**, *388–2396 (1993).*

14. Yuan, J., Gupta, V., and Pronin, A., "Measurement of Interface Strength by the Modified Laser Spallation Technique. III. Experimental Optimization of the Stress Pulse," J. Appl. Phys., **74,** *2405–2410 (1993).*

15. Barker, L. M. and Hollenbach, R. E., "Interferometer Technique for Measuring the Dynamic Mechanical Properties of Materials," Rev. Sci. Instrum., **36**, *1617 (1965).*

16. Wang, J., Weaver, R.L., and Sottos, N.R., "A Parametric Study of Laser Induced Thin Film Spallation," EXPERIMENTAL MECHANICS, **42** *(1), 74–83 (2002).*

17. Evans, A. and Hutchinson, J., "The Thermomechanical Integrity of Thin Films and Multilayers," Acta Metall. Mater., **43**, *2507–2530 (1995).*

18. Thouless, M.D., "Fracture of a Model Interface Under Mixed-mode Loading," Acta Metall., **38**, *1135–1140 (1990).*

19. Charalambides, P.G., Cao, H.C., Lund, J., and Evans, A.G., "Development of Test Method for Measuring the Mixed Mode Fracture Resistance of Bimaterial Interfaces," Mechanics of Materials, **8**, *269–283 (1990).*

20. Wang, J.S. and Suo, Z., "Experimental Determination of Interfacial Toughness Using Brazil-nut Sandwich," Acta Metall., **38**, *1279–1290 (1990).*

21. Graff, K., Wave Motion in Elastic Solids, Dover (1991).

22. Barker, L.M. and Hollenbach, R.E., "Shock Wave Studies of PMMA, Fused Silica and Sapphire," J. Appl. Phys., **41**, *4208–4226 (1970).*

23. Wang, J., "Thin Film Adhesion Measurement by Laser Induced Stress Waves," PhD thesis, University of Illinois at Urbana-Champaign (2002).

24. Hutchinson, J.W. and Suo, Z., "Mixed Mode Cracking in Layered Materials," Advances in Applied Mechanics, **29**, *63–191 (1992).*

